Spectrally Condensed Fluid Turbulence and L-H Transitions in Plasma[*)]

Michael SHATS and Hua XIA

Research School of Physics and Engineering, The Australian National University, Canberra, ACT, 0200, Australia

Recent experimental and theoretical studies of two-dimensional (2D) turbulence reveal that spectrally condensed turbulence which is a system of coupled large-scale coherent flow and broadband turbulence, is similar to plasma turbulence near the L-H transition threshold. Large condensate vortices fed *via* the turbulent inverse energy cascade, can control both the level of the broadband turbulence by shear decorrelation, and the energy injected into turbulence at the forcing scale *via* sweeping of the forcing-scale vortices. The interaction between these ingredients of spectrally condensed fluid turbulence is in many aspects similar to the interactions in the zonal flow-GAMs-turbulence system in plasma. In this paper we overview recent results on condensed 2D turbulence and present evidence of interaction between its three components: condensate structures, turbulence and forcing-scale vortices. This is compared with the modifications in the spectra of plasma electrostatic potential during L-H transitions. It is shown that mean zonal flows are spatially and temporally correlated with both the broadband turbulence and with the narrow spectral range identified as the spectral range of the underlying instability.

1. Introduction

Interaction between large-scale coherent structures and turbulence is a very important problem in geophysics, astrophysics, plasma physics and other areas. In many cases turbulence feeds coherent structures. On the other hand, turbulence is affected by coherent shear flows. Such a complex interplay between the two is rather difficult to describe theoretically. In this paper we overview our recent experimental studies in two-dimensional (2D) fluid turbulence and in magnetically confined plasma in the H-1 heliac.

Dual cascades of energy and enstrophy predicted by Kraichnan in 2D turbulence [1] lead to the spectral power of $E(k) = C_k \varepsilon^{2/3} k^{-5/3}$ for the wave numbers smaller than the wave number k_f of the forcing scale, $k < k_f$ (the inverse energy cascade range), and to $E(k) = C_q \eta^{2/3} k^{-3}$ for the small scales, $k > k_f$ (forward enstrophy cascade range). Here ε and η are the dissipation rates of energy and enstrophy correspondingly. These two ranges have been found in numerical simulations of the 2D turbulence and have also been confirmed in experiments. In homogeneous turbulence, spectral energy flux ε is expressed via the third-order moment of the velocity [2]: $S_3 = \left\langle (\delta V_L)^3 \right\rangle + \left\langle \delta V_L (\delta V_T)^2 \right\rangle = 2\varepsilon r$ with $\varepsilon > 0$ for an inverse cascade. Here δV denotes the difference of velocities at two points separated by distance r, angular brackets denote ensemble

averaging over realizations, and the subscripts denote the longitudinal (L) and transverse (T) velocity components relative to r.

It is often said that 2D turbulence has tendency to generate coherent structures due to the inverse energy cascade. Though this may be true for decaying turbulence, generally this is incorrect. In forced quasi-2D turbulence coherent structures appear as a result of spectral condensation in the presence of a boundary. In other words, this is a finite system size effect which requires that the linear (scale-independent) damping should be sufficiently small to allow energy transfer via inverse energy cascade to generate scales comparable to the system size. When this happens, a structure coherent across the system size develops and dominates the flow. Such coherent condensate is a shear flow which modifies underlying turbulence that feeds it. This new state, referred to as condensed turbulence presents particular interest to plasma physics.

Large-scale coherent flows interacting with the background turbulence are the focus of plasma turbulence research in magnetic confinement devices. Similarly to the spectrally condensed turbulence in fluids, zonal flows (ZF) in plasma are generated by turbulence and coexist with it forming dynamic ZF-turbulence system [3]. It is believed that ZF reduce turbulence and suppress turbulent transport of particles and energy across magnetic field leading to improved confinement, like H-mode. The details of the mechanisms through which this occurs are not fully clear, but there is strong evidence that shear decorrelation of tur-

bulence plays a key role.

Despite different nature of magnetically confined plasma and thin layers of fluids, comparative studies of spectrally condensed turbulence in quasi-2D flows and ZF-turbulence system in plasma appear to be productive and useful for both disciplines. In this paper we overview results of our studies of these systems with particular focus on the interaction between three systems' ingredients: condensate structure (ZF in plasma), broadband turbulence, and the forcing scale vortices (drift-wave instability in plasma).

2. Spectral Condensation in 2D Fluids

A good laboratory model of 2D turbulence can be reproduced experimentally in thin stratified layers of electrolyte by electromagnetically generating large number of quasi-2D vortices. Experimental setup is described in [4] and is shown schematically in Fig. 1. Turbulent flow is generated in stratified thin layers of electrolyte (NaCl water solution) resting upon heavier non-conducting fluid (Flourinert), each layer several millimeters thick. Turbulence is generated by forcing up to 900 $J \times B$-driven vortices in a cell. Spatially varying, vertically directed (normal to the fluid layers) magnetic field B is produced by a 30×30 matrix of permanent magnets placed under the bottom of the fluid cell in a checkerboard fashion. Solid Perspex square boundaries of various sizes are inserted to generate spectral condensate. Two carbon electrodes on the either side of the cell are used to run electric current across conducting layer to generate vortices which force turbulence. Flow is visualized using thin laser sheet (1 mm) parallel to the free surface. Laser light is scattered by imaging particles suspended in the top layer. Images of the particles are recorded using video camera from above. Shortly

after the current is switched on, forcing scale vortices are observed as seen in Fig. 2 (a) showing particle streaks at 3 different moments of the flow evolution.

As the forcing scale (9 mm) vortices interact with each other, larger eddies are formed due to the transfer of energy from smaller scales (inverse energy transfer), as in Fig. 2 (b). If the bottom damping is sufficiently low (this is controlled by changing the thickness of the bottom layer) the size of the largest eddies may become comparable to the boundary size and spectral energy starts accumulating in one big vortex, or spectral condensate, Fig. 2 (c). The threshold and conditions of spectral condensation are described in more detail elsewhere [5].

Here we focus on the mechanics of the formation of the coherent vortex and on the modifications caused by the vortex in the spectra of the underlying turbulence. First, coherent structures are transiently formed in the flow even before generation of a circular vortex. This is illustrated in Fig. 3. Vortices the size of about 1/4 of the box size

Fig. 2   Particle streaks photos at different stages of the flow evolution on the way to spectral condensation: (a) $t = 3$ s, (b) $t = 11$ s, (c) $t = 50$ s.
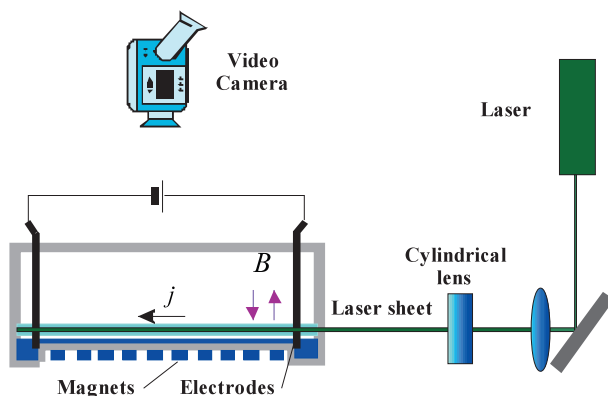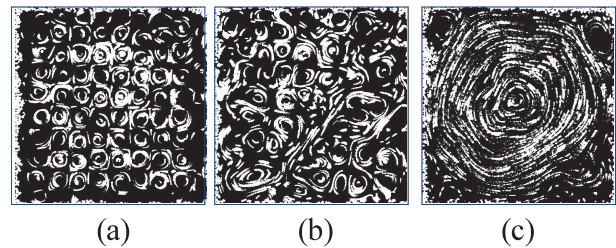

Fig. 1   Schematic of the experimental setup: imaging particles suspended in the top (conducting) layer are illuminated using thin laser sheet. Turbulence is produced by the interacting $J \times B$ driven vortices in the top layer. Linear damping is controlled by changing thicknesses of both fluid layers.
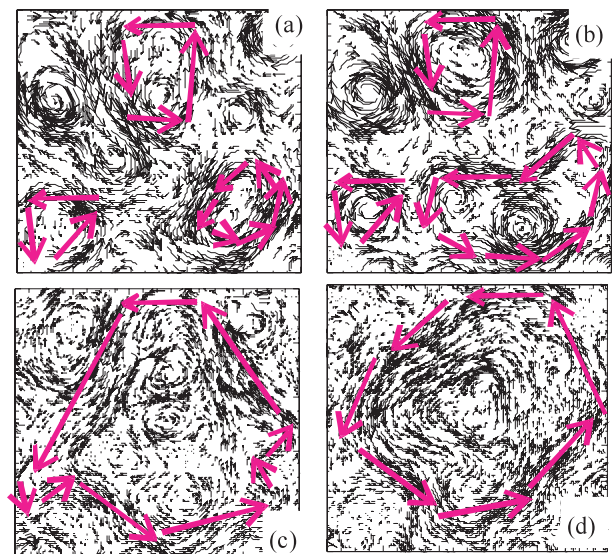

Fig. 3   Time-averaged velocity fields show the merger of the coherent same-sign vortices during the formation of the condensate vortex.
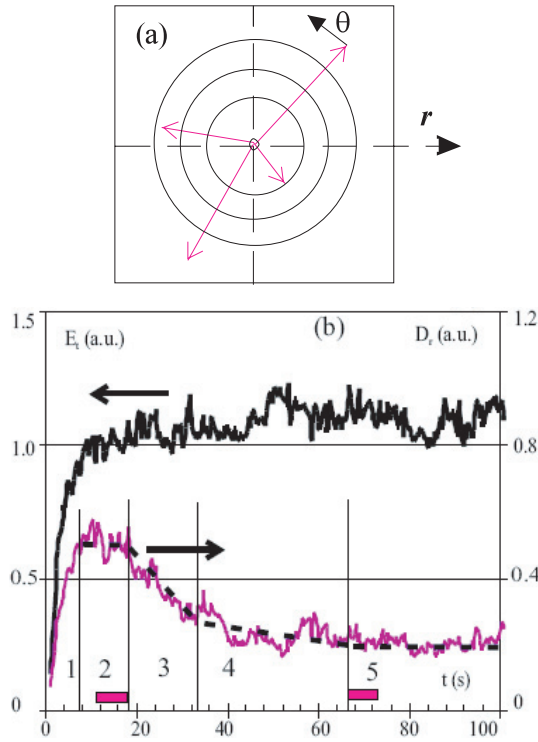
Fig. 4   (a) Polar coordinates with origin in the center of the condensate vortex. (b) Time evolution of the total kinetic energy (top) and of the radial diffusion coefficient (bottom) during spectral condensation of turbulence.

are formed. The same sign vortices then start destroying the separatrix between them until finally one "circular" vortex forms. The difference between large-scale turbulence eddies, such as those seen in Fig. 2 (b) and vortices of Fig. 3 (a, b) is the lifetime: a lifetime of a vortex is longer than the turnover time. Experimentally we reveal coherent vortices by time-averaging over many instantaneous velocity fields.

The merger of the vortices into a single circular flow leads to the regularization of turbulence. To qualitatively characterize transport of a passive scalar, which is of interest for comparison with plasma particle transport, we introduce polar coordinate system in the fluid cell, as shown in Fig. 4 (a). The center of it coincides with the center of the box, which is close to the center of the condensate vortex. In this system 2D velocity can be split into radial V_r, and azimuthal V_θ, components. Then transport of the passive scalar from the center of the box toward the boundary can be characterized by the radial diffusion coefficient

$$D_r = \frac{\langle \Delta r^2 \rangle}{\Delta t} = \frac{\Delta t^2 \langle \Delta V_r^2 \rangle}{\Delta t} = \Delta t \langle \Delta V_r^2 \rangle \qquad (1)$$

Here square brackets denote averaging over the boundary box.

Figure 4 (b) shows time evolution of the total kinetic energy of the flow E_t, and of the radial diffusion coefficient D_r. For the D_r evolution, four dynamic stages can

be identified. D_r grows fast during the stage (1), reaching its maximum and then stays constant during the stage (2). After that, D_r decreases rapidly, stage (3), then slowly, stage (4), until it reaches another steady state at $t \approx 65$ s. Total kinetic energy $E_t = 1/2\Sigma V^2$ increases rapidly during the stage (1) together with D_r, and then slowly grows until reaching its steady-state value during stage (4).

The merger of two co-rotating vortices in 2D fluid has been studied extensively (see e.g. [6,7]). It has been shown that an increase of the vortex radius is observed due to viscous diffusion of vorticity. This induces a simultaneous increase of the ratio between the vortex radius and the separation distance. This quantity also changes in the presence of a third vortex in the neighborhood of the vortex pair. In any case, vortices merge into a bigger vortex in a fast convective process when this aspect ratio reaches critical value. Though during the vortex evolution illustrated above, the vortices are not exactly the same size and the system is constantly forced, we observe qualitatively similar time evolution of the flow on the way to spectral condensation, Fig. 4 (b): formation of vortices during stage (1) (Fig. 3 (a)), their slow diffusive growth during stage (2) (Fig. 3 (b)), then fast convective merger during stage (3) followed by a slow symmetrization of the condensate during stage (4) (evolution from Fig. 3 (c) to (d)).

After the condensate vortex is formed, it exists in steady state. The energy is still supplied to it via the inverse energy cascade from the forcing scale. Properties of the underlying turbulence however change in the presence of spectral condensate. First, this coherent shear flow reduces the lifetime of the turbulent eddies via shear decorrelation mechanism [8].

Turbulence suppression by sheared flow [8] was proposed by plasma physicists as a hydrodynamic model aimed at explaining turbulence reduction near transport barriers which form in plasma in H-mode. Since then this concept has received wide recognition in the plasma community, but it remained virtually unknown in fluid dynamics until the first experimental proof in 2007 [4]. The mechanism of the shear suppression is as follows. When a turbulent eddy is placed in a stable flow whose velocity varies in the direction perpendicular to the flow direction, it becomes stretched and distorted. The shear suppression can be viewed as the reduction in the eddy's lifetime. It occurs when the inverse shearing rate $\tau_s \sim \omega_s^{-1}$ becomes shorter than the eddy turnover time, or its lifetime, τ_e whatever is shorter, providing that the interaction time between turbulence and flow is longer than other time scales. A reduction in the spectral power in the presence of a shear flow is due to the shortened correlation time of eddies. Dimensional scaling analysis which takes into account turbulent diffusion, shows that this shortened correlation time τ_{se} is related to the shear straining time and the eddy lifetime τ_e as $\tau_{se} = \tau_e^{1/3}\tau_s^{2/3}$ [8].

To study effects of the shear flow on turbulence one first needs to separate turbulent velocity fluctuations from
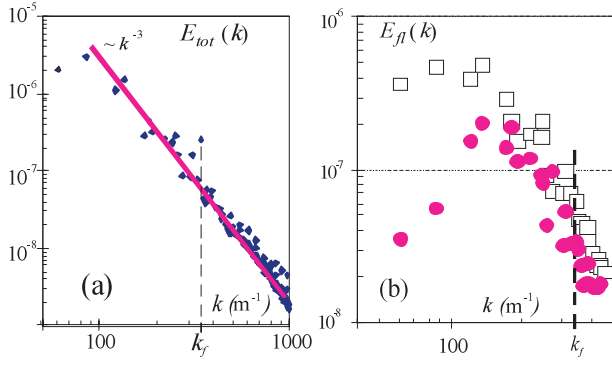
Fig. 5 (a) Kinetic energy spectrum of the total velocity field averaged over stage 2 of the flow evolution. (b) Spectra computed after the mean velocity subtraction during stages 2 (open squares) and 5 (solid circles).

mean flows. As shown in [5], the presence of the mean shear flows in the velocity fields changes all statistical moments of velocity. The mean flow is thus computed first by averaging over many realizations in time, then this time-average velocity field is subtracted from each instantaneous 2D velocity field to recover fluctuations: $\tilde{V}(x, y) = V(x, y) - \bar{V}(x, y)$. Figure 5 shows wave number spectra corresponding to two stages of turbulence evolution in Fig. 4 (b): stage (2) and stage (5). Left panel shows the kinetic energy spectrum measured at stage (2) without subtracting mean flow. This spectrum is close to the power law of $E(k) \sim k^{-3}$ both below and above the forcing wave number k_f. Right panel shows energy spectra after mean subtraction, during stage (2) (squares), and stage (5) (solid circles), corresponding to strong circular condensate.

Mean subtraction recovers spectra of the underlying turbulence. In the presence of the condensate vortex spectral energy of the large-scale turbulent eddies at $k < 160\,\mathrm{m}^{-1}$ is reduced. This agrees with the shear decorrelation criterion $\omega_s \tau_e > 1$. As explained in [4], since $\omega_s = l\left[(1/r)(\mathrm{d}V_\theta/\mathrm{d}r) - V_\theta/r^2\right] = sl$, shear decorrelation is more efficient for the larger-scale eddies, $\omega_s \tau_e \sim l^{5/3}$. Indeed, for the conditions of the described experiment, the shear decorrelation criterion is satisfied for the scales $l > 22\,\mathrm{mm}$, which corresponds to the wave number range $k = \pi/l < 145\,\mathrm{m}^{-1}$. It is in this range, where spectral energy of the fluctuations are noticeably reduced, as seen in Fig. 5 (b).

Shear decorrelation is not the only mechanism through which a mean flow can affect turbulence. In the described experiments energy is injected into the flow by constantly $\boldsymbol{J} \times \boldsymbol{B}$-driven vortices. These vortices are generated at fixed spatial locations corresponding to the positions of the permanent magnets. When the mean flow velocity becomes large, these forcing-scale vortices are swept away from their initial positions such that the energy injected via $\boldsymbol{J} \times \boldsymbol{B}$ force is reduced. To model this, a mean flow was imposed externally by using large magnetic dipole close to
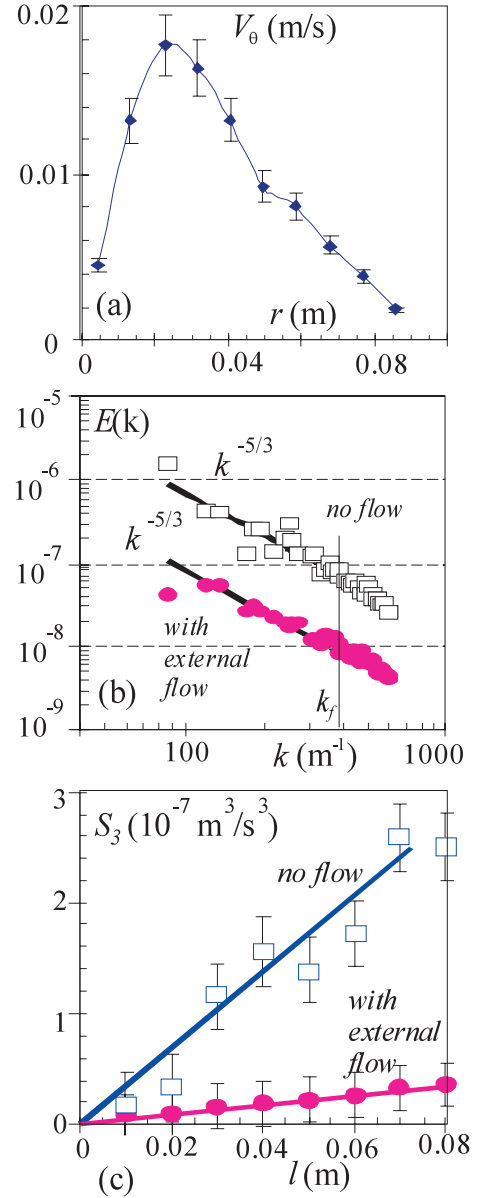

Fig. 6 (a) Radial profile of the azimuthal velocity component of the flow externally imposed on top of developed turbulence. (b) Kinetic energy spectra computed after subtracting mean flow: without imposed mean flow (open squares) and with imposed flow (circles). (c) 3rd order structure functions of the velocity fluctuations as a function of the separation distance l: without imposed flow (open squares) and with the flow (circles).

the free surface of the current-carrying fluid layer. Strong circular flow, similar to the vortex forming during spectral condensation, is characterized by its azimuthal velocity component shown in Fig. 6 (a) as a function of its radius. After the mean velocity is subtracted, the kinetic energy spectrum is modified in the presence of the imposed flow as shown in Fig. 6 (b). The spectral energy is reduced everywhere in the inertial range of the inverse energy cascade, including the forcing scale k_f. Such modifications in the spectrum are consistent with the expected reduction in the

energy flux forced at $k = k_f$ and cascading toward smaller k. This energy flux ε can also be estimated using the Kolmogorov law from the ensemble averaged third-order velocity moment S_3, as described in [4]: $\varepsilon = S_3/r$, where $S_3(l) = \langle \delta V^3 \rangle$ is the 3rd-order structure function, or the mean cube of the velocity increment for all points in the flow separated by distance l. Figure 6 (c) shows S_3 as a function of l before (squares) and after the external flow is applied (circles). First, the $S_3(r)$ dependence is linear, suggesting an almost constant energy flux ε in the inertial range. Second, this flux (which equals to the energy production and to the energy dissipation rates in steady state) is reduced in the presence of imposed flow by almost a factor of 10. This leads to the reduction in the spectral energy of Fig. 6 (b).

Sweeping of the forcing-scale vortices affects energy input into turbulence when the sweeping rate $\omega_{sw} = V_\theta/l$ exceeds the forcing scale vortex turnover time, $\omega_{sw}\tau_e > 1$. Unlike shearing, which acts more efficiently on larger scales, sweeping affects smaller scales first, since $\omega_{sw}\tau_e \propto V_\theta(\varepsilon l)^{-1/3}$.

Thus we identify two different mechanisms through which a mean large-scale flow affects underlying turbulence. The flow leaves a clear "footprint" on the turbulence spectra: a suppression of the lower-k spectral range in case of shear decorrelation of turbulent eddies, and the reduction in the spectral energy in the entire inertial range, but without the change in the spectrum power-law of $E \sim k^{-5/3}$ when the sweeping is the dominant mechanism. And, of course, mean flows can lead to the combination of both effects, affecting the shape of the spectrum as well as the energy injection [4].

Spectral condensation of quasi-2D turbulence presents an interesting example of the self-regulation of turbulence. One can argue, that even in the limit of a very low damping of the large-scale flow, the condensate vortex controls the energy flux delivered via the inverse energy cascade. The accumulation of the spectral energy in the condensate which leads to its growth, will eventually result in sweeping of the forcing scale vortices, the reduction on the energy flux in the inertial range, and to the saturation of the condensate vortex energy. Similarly, the shear decorrelation of the larger-scale turbulent eddies will arrest the inverse energy cascade and will also lead to the stabilization of the condensate energy.

3. Zonal Flows and Turbulence in Plasma

Zonal flows and their interaction with turbulence were studied in the context of L-H transitions in the H-1 heliac. The plasma parameters were in the range: electron temperature $T_e = 10\text{-}20$ eV, electron density $n_e < 2 \times 10^{18}$ m^{-3}. For more details see [9]. Fluctuations in the electron density and electrostatic potential were studied using various combinations of the Langmuir probes, which were inserted
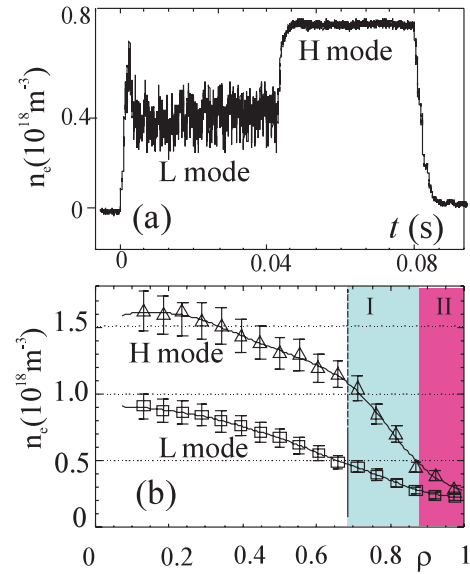

Fig. 7 (a) Time evolution of the line-average electron density during spontaneous L-H transition. (b) Radial profiles of the electron density in L (open triangles) and H (squares) confinement modes.

into plasma as deep as the magnetic axis. Zonal flows and turbulent fluctuations were studied in the conditions close to the L-H transition threshold: either just above, or just below the threshold, or during plasma discharges showing spontaneous transitions, like the one illustrated in Fig. 7. Particle confinement typically doubles during the transition leading to higher electron density, Fig. 7 (a). Radial profiles of electron density in H-mode develop a characteristic kink at $\rho \approx 0.7$, which marks the position of the transport barrier, Fig. 7 (b). Fluctuations in the electrostatic potential and in the electron density are substantially reduced from L to H-mode.

The frequency spectra of the potential fluctuations at the transport barrier are modified during the transition as shown in Fig. 8. Frequency spectra carry information about the wave number spectra. In the laboratory frame of reference, frequencies of the fluctuations are Doppler shifted due to the presence of the $E \times B$ drift: $\omega_{lab} = \omega_{plasma} + k_\theta V_{E \times B}$. The $E \times B$ drift often dominates over the phase velocity in the plasma frame. In this case the fluctuation frequencies in the lab frame are proportional to poloidal wave numbers. Since in the broadband turbulence the wave number spectra are usually isotropic, $k_\theta \approx k_r$ one can assume that $k \approx \sqrt{2}k_\theta \propto \omega$. The $E \times B$ Doppler shift plays in such cases a role of the wave number spectrograph.

In L-mode, a spectrum of the potential fluctuations typically shows two power laws: $P \sim f^{-5}$ at $f > 30$ kHz and $P \sim f^{-3.6}$ at $f < 30$ kHz, Fig. 8 (a). Previously, the spectral transfer analysis of the potential fluctuations in H-1 identified the spectral range of $f_i = (25\text{-}30)$ kHz as the range of the unstable drift wave [10], which is analogous to the forcing-scale wave number in 2D fluid. In H-
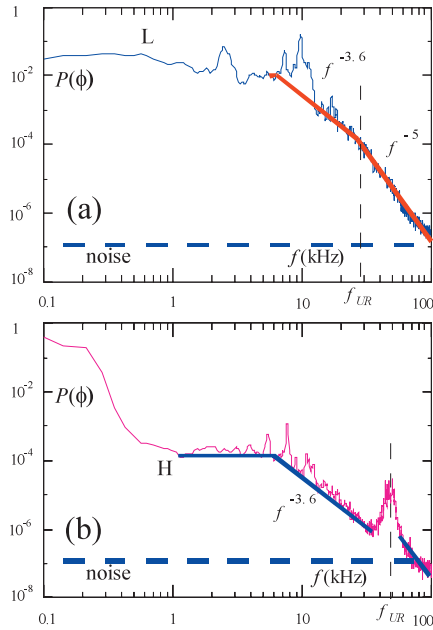
Fig. 8 Power spectra of the fluctuations in the floating potential measured at the transport barrier at $\rho \approx 0.7$ in (a) L-mode and (b) H-mode.

Fig. 9 Radial profiles of (a) electron density and (b) spectral power density of the low-frequency ($f_1 = (0.5 \pm 0.3)$ kHz) zonal flow in H-mode

mode, these two power laws are also observed, Fig. 8 (b), but the cross-over is Doppler shifted toward higher frequency, $f_i = (50\text{-}90)$ kHz due to the higher radial electric field. As it has been previously discussed [10], the broadband turbulence in H-1 is in several aspects similar to the Hasegawa-Mima type turbulence. In particular, the phase shift between the potential and density fluctuations is close to zero. The two power laws in the frequency spectra seen in Fig. 8 are also consistent with the results of numerical simulations of the Hasegawa-Mima turbulence which give [11–13]: $E(k) \propto k^{-11/3}$, $k < k_f$, and $E(k) \propto k^{-5}$, $k > k_f$. These power laws are predicted for the conditions when $k_f \rho_s \ll L_n/\rho_s$. Here L_n is the density scale length and ρ_s is the ion Larmor radius taken with electron temperature. The observed power laws of $P \sim f^{-3.6}$ in the inverse energy cascade range and $P \sim f^{-(5 \div 6)}$ are close to those expected for the Hasegawa-Mima spectra.

Another interesting feature of the spectrum modification during the L-H transition, is that simultaneously with the strong reduction in the fluctuation level in the frequency range $f > 1$ kHz, the low-frequency feature at $f < 1$ kHz is increased in H-mode, Fig. 8 (b).

This low frequency band has been identified as the mean-zero-frequency zonal flow which has poloidal and toroidal mode number of $m = n = 0$ [14]. The radial profile of the spectral power density of the mean ZF is maximum near the transport barrier [9]. This is shown in Fig. 9 where the spectral power of the mean ZF is plotted as a function of plasma radius. It has been suggested that mean ZF may be responsible for locally reducing the particle transport at the transport barrier position [9]. Moreover, the radial re-
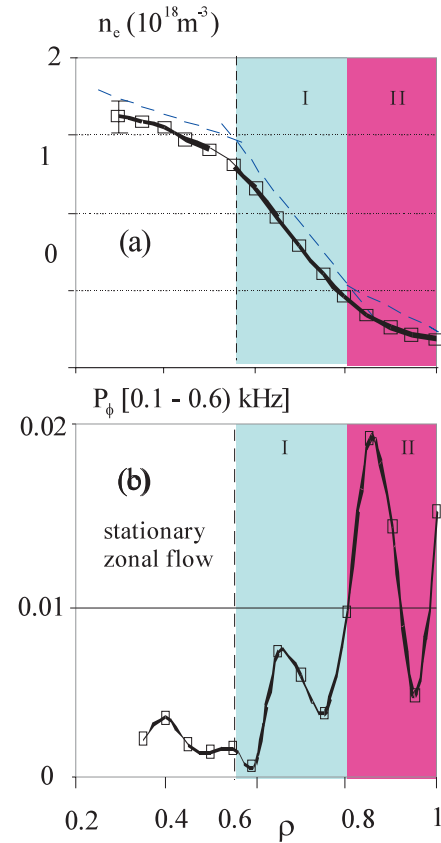
gion in plasma where mean ZF develops in H-mode is very close to the radius at which finite-frequency zonal flows, or geodesic acoustic modes (GAM) are maximum in L-mode, prior to L-H transition [15]. Recently, such a link between GAM and mean ZF has been demonstrated in the dynamics studies of the L-H transitions in the D-IIID tokamak [16].

A spectral range of the unstable drift wave at $f \approx f_i$ appears to be coupled to the mean ZF. Such coupling is best characterized using the amplitude correlation function (ACF) used in these studies [14]. The ACF measures the degree of correlation between two frequency bands within the same signal. Here we are interested in studying the coupling between the mean low-frequency ZF band of $f_1 = (0.5 \pm 0.3)$ kHz and the unstable drift range band of $f_2 = (57.6 \pm 0.3)$ kHz. Two time series are extracted from the potential fluctuation signal by band-pass-filtering f_1 and f_2. These two time series are then squared and passed through a low-pass filter to obtain only the slow varying amplitude information. Then the cross-correlation function between these signals is computed, to obtain the amplitude correlation function, ACF,

$$ACF(\tau) = \left\langle \left[x_1^2(t) \right] \left[x_2^2(t+\tau) \right] \right\rangle \qquad (2)$$

Figure 10 (a) shows the spectrum of the potential fluctuations measured in H-mode inside the transport barrier
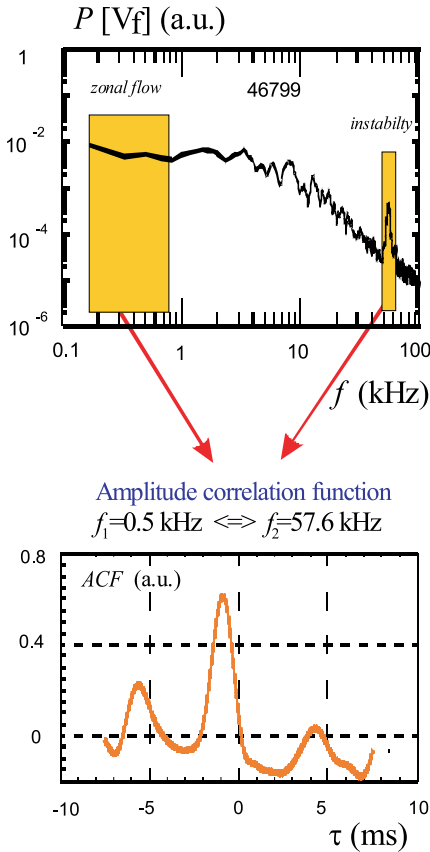
Fig. 10 (a) Power spectrum of the floating potential fluctuations in H-mode at $\rho \approx 0.5$. (b) Amplitude correlation function measured between the frequency bands $f_1 = 0.5$ kHz and $f_2 = 57.6$ kHz. The width of each band is $\Delta f = 0.6$ kHz.
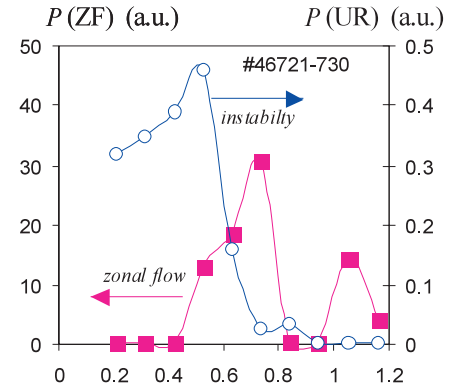

Fig. 11 Spectral power densities of the mean ZF (solid squares) and the fluctuation in the unstable range (circles) as functions of the normalized plasma radius $\rho = r/a$, where a is the mean minor plasma radius.

at $\rho \approx 0.5$. Two boxes indicate frequency bands used to compute the ACF. The two bands are strongly coupled showing the correlation above 0.6. It should be noted that the correlation of the ZF band with other frequencies in the spectrum, $f < f_i$ does not exceed 0.4 at this radial position.

Spectral power densities of the mean ZF and of the unstable range (UR) are anti-correlated in space in H-mode. Figure 11 shows radial profiles of the ZF, $P_{f1}(\rho)$, and of the fluctuations in the unstable range, $P_{f2}(\rho)$. The maximum of the UR, P_{f2}, is observed at $\rho \approx 0.5$, while further out, in the region of the transport barrier, it is reduced by a factor of 10. This sharp drop in the intensity of the UR fluctuations is correlated with the 3-fold increase in the spectral power of the mean ZF.

The character of the spectral coupling between ZF and the other frequencies in the broadband spectrum also changes in the transport barrier region. While at $\rho \approx 0.5$ the only two strongly coupled frequency bands are those of ZF and UR (as in Fig. 10), in the transport barrier, where mean ZF is strong, the value of the ACF between $f_1 = (0.5 \pm 0.3)$ kHz and all other frequencies in the spectrum is above 0.5, suggesting strong coupling of the ZF to all frequencies. How this can be interpreted? Using the

analogy with the mechanism of sweeping of the forcing scale vortices in 2D fluids described in Sec. 2, it is possible to speculate that mean ZF which is spectrally coupled to the UR via the inverse cascade of energy from UR to ZF on one hand, and via the sweeping of the UR waves by the ZF field. In this case, when the ZF becomes sufficiently strong, it may modulate the UR and the energy flux in the inertial range. This would lead to the apparent coupling between all the frequencies in the inertial range and mean ZF.

4. Summary

Experimental studies of interaction between large-scale coherent flows in thin fluid layers and in magnetically confined toroidal plasma show several common features. In both systems the inverse energy cascade delivers energy from the forcing scale (unstable drift wave range) into the broadband turbulence. In fluids, this energy may accumulate at the scale comparable to the system size which leads to spectral condensation and generation of the large-scale vortex. In plasma, broadband turbulence is also generated via the inverse energy cascade [10]. The inverse cascade may be responsible for delivering spectral energy into a zonal flow. In L-mode it is accumulated in GAM [14], while in H-mode the GAM dominance turns into the dominance of the mean zonal flow.

It is not clear how mean ZF are sustained in H-mode. The fluctuation spectra in H-mode show the power laws expected in the energy and the potential enstrophy inertial ranges, Fig. 8 (b), which may be indicative of the inverse energy cascade spectral transfer from the higher frequency unstable range. A strong link between the two spectral ranges is also evident from the spatial (anti-)correlation between UR and ZF of Fig. 11. On the other hand, strong spectral coupling between the unstable range fluctuations and mean zonal flow, Fig. 10, maybe indicative of the non-local energy transfer from UR to ZF via modulational in-

stability [17]. The result of Fig. 11 is also consistent with the idea of the Reynolds stress driven ZF, since the maximum of ZF is observed close to the radial gradient of the drift wave intensity.

The presence of strong mean zonal flow, which in the spectra is observed as the spectrally broadened feature with $f_1 = 0 \pm \Delta f$, may lead to the modulation of the spectral energy flux in the inertial range. This may explain strong spectral coupling (high values of ACF) between ZF and the broadband turbulence in H-mode.

In thin fluid layers, we also observe a mixture of local spectral transfer due to the inverse energy cascade, and non-local interaction between coherent condensate vortex with the forcing scale. In this system the condensate vortex affects energy injection into inertial range via sweeping of the forcing scale vortices. It also decorrelates larger scale turbulent eddies and modifies the spectrum of the broadband turbulence. This effect was first proposed to explain plasma confinement effects [8] and recently was shown to exist in 2D fluids [4].

We should stress that though the above comparative studies of spectrally condensed turbulence in thin fluid layers and in magnetically confined plasma (proposed in [18]) are useful as an inspiration for a first-principle interpretation of the plasma results, this approach cannot possibly explain rich variety of effects observed in toroidal plasma (see e.g. [19] and references therein). The generation of zonal flows does not generally require the inverse energy cascade as the energy transfer mechanism into zonal flows. Parametric-modulational instability of drift waves can lead to the generation of a low-frequency sideband, or a zonal flow [3]. This mechanism of the zonal flow formation has recently been confirmed and systematically studied in cylindrical plasma [20]. The formation of a zonal flow as a result of modulational instability has also been observed in the H-1 heliac [21] where the growth of the $k_\theta \approx 0$ low frequency structure was found to be correlated with the modulation of a coherent parent wave. The modulational-instability-driven zonal flows are particularly likely to develop in H-mode, where levels of the broadband turbulence are substantially reduced.

The quasi-two-dimensionality of the plasma turbulent flow in this case is not strictly necessary (no need for the inverse energy cascade). The generation of the large-scale shear flow can also be similar to the processes in rotating fluids. Numerical simulations of turbulence in a rotating

frame found that the large-scale two-dimensional vortices are generated even though the forcing was 3D [22]. It was suggested that the energy in this case was transferred directly from 3D modes into 2D modes, rather than the due to inverse local cascade process. In the plasma context, a similar result was obtained theoretically. As discovered in [23], the inverse energy transfer may occur due to near-resonant interactions of anisotropic trapped electron drift waves. In this case the spectral energy condenses into zonal modes.

[1] R.H. Kraichnan, Phys. Fluids **10**, 1417 (1967).
[2] A.S. Monin and A.M. Yaglom, *Statistical Fluid Mechanics* (MIT, Cambridge, Mass., 1975) Vol. 2.
[3] P.H. Diamond, S.-I. Itoh, K. Itoh and T.S. Hahm, Plasma Phys. Control. Fusion **47**, R35 (2005).
[4] M.G. Shats, H. Xia, H. Punzmann and G. Falkovich, Phys. Rev. Lett. **99**, 164502 (2007).
[5] H. Xia, H. Punzmann, G. Falkovich and M.G. Shats, Phys. Rev. Lett. **101**, 194504 (2008).
[6] P. Meunier, U. Ehrenstein, T. Leweke and M. Rossi, Phys. Fluids **14**, 2757 (2002).
[7] C. Cerretelli and C.H.K. Williamson, J. Fluid Mech. **475**, 41 (2003).
[8] H. Biglari, P.H. Diamond and P.W. Terry, Phys. Fluids B **2**, 1 (1990).
[9] H. Xia, M.G. Shats and H. Punzmann, Phys. Rev. Lett. **97**, 255003 (2006).
[10] H. Xia and M.G. Shats, Phys. Plasmas **11**, 561 (2004).
[11] M. Ottaviani and J.A. Krommes, Phys. Rev. Lett. **69**, 2923 (1992).
[12] N. Kukharkin, S.A. Orszag and V. Yakhot, Phys. Rev. Lett. **75**, 2496 (1995).
[13] T. Watanabe, H. Fujisaka and T. Iwayama, Phys. Rev. E **55**, 5575 (1997).
[14] M.G. Shats, H. Xia and M. Yokoyama, Plasma Phys. Control. Fusion **48**, S17 (2006).
[15] H. Punzmann and M.G. Shats, Phys. Rev. Lett. **93**, 125003 (2004).
[16] G. McKee, APS, 49th Ann. Meeting of DPP, YI1.004 (2007).
[17] A.I. Smolyakov, P.H. Diamond and V.I. Shevchenko, Phys. Plasmas **7**, 1349 (2000).
[18] M.G. Shats, H. Xia and H. Punzmann, Phys. Rev. E **71**, 046409 (2005).
[19] A. Fujisawa, Nucl. Fusion **49**, 013001 (2009).
[20] Y. Nagashima, S.-I. Itoh, S. Shinohara *et al.* Phys. Plasmas **16**, 020706 (2009).
[21] M. Shats and W. Solomon, New J. Phys. **4**, 30 (2002).
[22] L. Smith and F. Waleffe, Phys. Fluids **6**, 1608 (1999).
[23] P.W. Terry, Phys. Rev. Lett. **93**, 235004 (2004).